Consequences of superfluidity on the expansion of a rotating Bose-Einstein condensate: a numerical study

Egilea / Autor:
Eneko Mateos Madinabeitia
Zuzendaria / Director:
Michele Modugno
Zuzendarikidea / Co-Director:
Joanes Lizarraga

Contents

Introduction

Bose-Einstein Condensation (BEC) is a phenomenon that emerges at very low temperatures with bosonic particles. These particles are defined as having integer spin values, must have symmetric wave-functions under interchange of particles and obey Bose-Einstein statistics. Bosons may be fundamental particles that mediate the fundamental forces such as photons or they can also be bigger particles like bosonic isotopes of atoms such as Helium, Sodium or Rubidium. Unlike Fermions, they do not obey the Fermi exclusion principle, and therefore they are free to occupy the same quantum state [1]. This way, the the condensate becomes a macroscopic state of matter in which quantum phenomena become apparent.

One of such quantum characteristics is superfluidity, and it was first theorized for liquid Helium at almost the absolute zero ($0\ K$). Superfluids exhibit several unique features such as zero viscosity, which means that they can flow without any resistance, or quantised vortices, which implies certain discrete allowed values for the circulation around a region with an absence of superfluids [2].

In the 1920s, Satyendra Nath Bose [3] and Albert Einstein [4] theorized about this kind of occurrence in an ideal (uniform and non interacting) bosonic gas, but the existence of the BEC was not experimentally verified until 1995, when Eric Cornell, Carl Wieman, and Wolfgang Ketterle successfully produced a condensate using ultra-cold alkali metal atoms; specifically ^{87}Rb in the case of Cornell and Wieman [5], and ^{23}Na for Ketterle [6]. They were awarded the Nobel Prize in 2001 for these findings.

There are a few principles that permit the existence of this condensate. First of all, the particles with an integer spin obey Bose-Einstein statistics and can occupy the same quantum state. Secondly, particles at extremely low temperatures occupy the lowest energy level of a given system due to their low thermal energy. Because of that, the wavefunctions of these particles start behaving in a coherent way, so we are able to describe them with a single wave-function that, in fact, describes the matter distribution of the atoms in the condensate.

This state of matter is specially optimal to observe phenomena such as superfluidity or quantised vortices, and it is useful to simulate quantum states or do interferometry [7]. Besides, it is relatively easy to manipulate condensates using lasers or magnetic traps, and hence, they represent a good platform to study said quantum events.

The main goal of this thesis is to numerically simulate the free expansion a rotating Bose-Einstein condensate, in order to analyze the effects of superfluidity. A non-rotating Bose-Einstein condensate in a *cigar* shape created by the axial symmetry of the trapping potential expands very differently from a usual thermal cloud: instead of reaching a

spherical symmetrical configuration, the BEC will expand from the short axis much faster than from the long axis, so after passing a symmetrical shape, the original short axis will be the expanded one. If the condensate is rotating, then the moment of inertia is quenched with respect to the rigid body value. The important consequence of it is that due to the conservation of energy and angular momentum, the moment of inertia cannot be zero and therefore during the evolution the condensate can never pass through a symmetric (circular) configuration. Instead a rapid rotation of the long and short axes is performed when close to the forbidden configuration and the BEC continues to expand from the initial long axis instead of the initial short one.

We will also compare the rotating condensate with simulations of thermal clouds over the critical temperature needed to create the BEC and simulations of non-rotating condensates, so that we can see the differences compared to the main objective of the thesis.

This work is divided in four chapters, plus a concluding section and an Appendix. In the first part a theoretical introduction to Bose-Einstein condensates will be made, specifically mentioning the Gross-Pitaevskii theory and the Thomas-Fermi approximation. In the second chapter, the method for solving the equations numerically will be introduced. In the third chapter a theoretical hypothesis will be made of how each case will evolve, and in the last chapter the results of different simulations will be described and compared. Lastly, the key conclusions will be stated about the work done. At the end, some mathematical derivations will be developed and numerical methods will be explained which are useful both in the second chapter and in the numerical resolution of the problem in hand. This last part will also include code snippets to ease the replication of simulations.

Chapter 1

Theory of Bose-Einstein condensation

In this chapter, we provide a general discussion of basic concepts of Bose-Einstein condensation in order to study the expanding gas. This discussion is inspired mainly on the following sources: [8], [9], [10], [11], [12].

1.1 The non-interacting BEC

We are interested in studying a system of ultra-cold bosons trapped in an external magnetic potential, and in order to do that, we will first analyze the situation in which the particles do not interact with each other.

Although there are many possibilities for the external potential, a usual way to trap the atoms is by using a quadratic potential, similar to a harmonic oscillator potential, which may be different in every direction. Therefore, for a system of N particles with mass m, the trapping potential considered will be,

$$V_{ext}(\boldsymbol{r}) = \frac{1}{2}m\left(\omega_x x^2 + \omega_y y^2 + \omega_z z^2\right) = \frac{1}{2}m\sum_{i=1}^{3}\omega_i r_i^2. \tag{1.1}$$

Using the previous potential, the Hamiltonian of the system is expressed as follows,

$$H = \sum_{j=1}^{N} H_j, \tag{1.2}$$

where H_i is the harmonic oscillator Hamiltonian for a single particle,

$$H_j = -\frac{\hbar^2}{2m}\nabla_j^2 + V_{ext}(\boldsymbol{r}_j). \tag{1.3}$$

It is known that the energy spectrum of the Hamiltonian for each individual boson, since particles are not interacting, is the following,

$$\varepsilon_{n_x,n_y,n_z} = \hbar\omega_x\left(n_x + \frac{1}{2}\right) + \hbar\omega_y\left(n_y + \frac{1}{2}\right) + \hbar\omega_z\left(n_z + \frac{1}{2}\right), \tag{1.4}$$

where $n_i = 0, 1, ...$

Due to the bosonic nature of the particles we are working with, the general wave-function $\Psi(\boldsymbol{r}_1, ..., \boldsymbol{r}_n)$ has to be symmetric when two components are interchanged, i.e. $\boldsymbol{r}_i \leftrightarrow \boldsymbol{r}_j$, and all bosons will occupy the ground state of the harmonic oscillator if $T = 0$. Therefore, we can express the many-body wave-function as a Hartree product of individual wave-functions,

$$\Psi(\boldsymbol{r}_1, ..., \boldsymbol{r}_n) = \prod_{j=1}^{N} \psi_0(\boldsymbol{r}_j), \tag{1.5}$$

where the individual wave-functions are the following,

$$\psi_0(\boldsymbol{r}) = \left(\frac{m\omega_{ho}}{\pi\hbar}\right)^{3/4} e^{-\frac{m}{2\hbar}\left(\omega_x x^2 + \omega_y y^2 + \omega_z z^2\right)}. \tag{1.6}$$

The harmonic oscillator frequency $\omega_{ho} = \sqrt[3]{\omega_x \omega_y \omega_z}$ is the geometric average of the oscillator frequencies.

Since bosons follow Bose-Einstein statistics, from a statistical-mechanical point of view the system can be described with a grand-canonical ensemble, in which

$$N = \sum_{n_x n_y n_z} \frac{1}{e^{\beta\left(\varepsilon_{n_x n_y n_z} - \mu\right)} - 1}, \tag{1.7}$$

where N is the total amount of particles, μ is the chemical potential and $\beta = 1/kT$. This predicts a critical temperature T_C that corresponds to the maximum temperature at which there are sufficient particles in the ground state energy so that there is a macroscopic occupation. In the case of a harmonic potential, we define N_0 as the number of particles in the ground state. With that, if we let the chemical potential $\mu = (3/2)\omega_{ho}$, which is when the number of particles in the ground state becomes macroscopic, we may rewrite Eq. (1.7) as

$$N - N_0 = \sum_{n_x, n_y, n_z \neq 0} \frac{1}{e^{[\beta\hbar(\omega_x n_x + \omega_y n_y + \omega_z n_z)]} - 1}. \tag{1.8}$$

Since the energy level gaps grow smaller when $N \to \infty$, we can replace the sum with an integral, and evaluating that integral yields

$$N - N_0 = \zeta(3) \left(\frac{kT}{\hbar\omega_{\text{ho}}}\right)^3, \tag{1.9}$$

where $\zeta(x)$ is the Riemann zeta function. To calculate the critical value, we let $N_0 = 0$, so we obtain the following equality:

$$kT_c = \frac{\hbar\bar{\omega}N^{1/3}}{\zeta(3)^{1/3}} \approx 0.94\hbar\omega_{ho}N^{1/3}. \tag{1.10}$$

If the collection of atoms is at a temperature higher than the critical one, we would consider there is no condensate but a thermal cloud with no properties that are characteristic to the BEC. Nevertheless, for the purposes of this work, we are going to consider the ground state of a perfect BEC as our initial condition; so we will take $T = 0$, therefore

$N_0 = N$, and the normalization condition the many-body wave-function needs to satisfy is

$$\psi(\boldsymbol{r}) = \sqrt{N}\psi_0(\boldsymbol{r}) \longrightarrow \int_{\mathbb{R}^3} |\psi(\boldsymbol{r})|^2 d\boldsymbol{r} = N. \tag{1.11}$$

From that equation we can deduce that the density distribution of the non-interacting condensate is

$$n(\boldsymbol{r}) = |\psi(\boldsymbol{r})|^2 = N|\psi_0(\boldsymbol{r})|^2. \tag{1.12}$$

It can be seen that the density scales linearly with N, even though the size of the condensate in each direction does not depend on it,

$$R_{0_j} = \frac{a_{ho_j}}{\sqrt{2}}, \quad a_{ho_j} = \sqrt{\frac{\hbar}{m\omega_j}}. \tag{1.13}$$

Therefore, a non interacting BEC can be characterized by the trapping potential ω_j. For some experimental insight, the characteristic length scale a_{ho} is usually of the order of microns, and $\hbar\omega_{ho}$ is of the order of nanokelvins.

1.2   Mean-field theory for an interacting condensate

Even though the previous discussion has been interesting from a theoretical point of view, in reality particles interact with each other, so in this section we will analyze the situation in which a Hartree approximation can be made with the mean-field g. The mean-field energy is used in various many-body systems to represent the average interaction energy between the particles of the system. It captures the dominant interaction neglecting small details for individual particles, and therefore it provides an interesting simplification from the complex potentials we have for each boson in the system, while maintaining good overall approximations. If we use the momentum representation $\psi(\boldsymbol{p})$ of the wave-function the mean-field will be a constant, but not in our spatial representation.

There are two conditions to be met for this approximation to be valid:

- The probability of finding two particles in the characteristic range r_0 of the inter-particle interactions has to be much lower than the average distance between the particles d, namely $d \gg r_0$. This is called the diluteness condition and holds even in classical situations.

- The thermal wavelength of particles, $\lambda_T = \sqrt{2\pi\hbar^2/(mk_BT)}$, has to be much larger than the interaction range in order to average the effects of said interactions. When λ_T is sufficiently large, the details of the interactions do not matter that much so the particle feels an average effect of the potential. This is due to the position of quantum particles not being defined perfectly but spread over a distance proportional to their thermal wavelength.

In this case, the initial wave-function will not change from the previous section, Eq. (1.5), but the Hamiltonian changes to

$$H = \sum_{i=1}^{N} \left[\frac{\boldsymbol{p}_i^2}{2m} + V_{ext}(\boldsymbol{r}_i) \right] + g\sum_{i<j} \delta(\boldsymbol{r}_i - \boldsymbol{r}_j), \quad g = \frac{4\pi\hbar^2 a}{m}, \tag{1.14}$$

where a is the s-wave scattering length of bosons. Keep in mind this is an approximation, and that the real potential $V(\boldsymbol{r}_{ij})$ would be made up of all interactions between the particle being solved for and all other particles in the BEC. That would not be possible to solve analytically and would be computationally expensive to approach; besides, the approximation proposed gives a really good picture of the condensate.

Once the Hamiltonian has been set, the energy of the system can be written as

$$E\left[\psi\right] = N \int d\boldsymbol{r} \left[\frac{\hbar^2}{2m}|\boldsymbol{\nabla}\psi(\boldsymbol{r})|^2 + V_{ext}(\boldsymbol{r})|\psi(\boldsymbol{r})|^2 + \frac{(N-1)}{2}g|\psi(\boldsymbol{r})|^4\right]. \qquad (1.15)$$

Notice how the interaction potential term is divided by 2 to avoid counting each interaction twice. Moreover, taking into account that $N \gg 1$, we can rewrite the energy of interaction as the following:

$$E = \frac{N(N-1)}{2V}g \approx \frac{1}{2}Vn^2g, \qquad (1.16)$$

and we can neglect the terms containing $1/N$ due to the large volume of particles in the BEC. Therefore, Eq. (1.15) becomes

$$E\left[\psi\right] = \int d\boldsymbol{r} \left[\frac{\hbar^2}{2m}|\boldsymbol{\nabla}\psi(\boldsymbol{r})|^2 + V_{ext}(\boldsymbol{r})|\psi(\boldsymbol{r})|^2 + \frac{1}{2}g|\psi(\boldsymbol{r})|^4\right]. \qquad (1.17)$$

Consequently, if we take the functional derivative of the expression above to minimize the energy, we arrive to the known Gross-Pitaevskii (GP) equation:

$$\frac{\delta E}{\delta\psi^*} = i\hbar\frac{\partial}{\partial t}\psi(\boldsymbol{r},t) = \left[-\frac{\hbar^2}{2m}\nabla^2 + V_{ext}(\boldsymbol{r}) + g|\psi(\boldsymbol{r},t)|^2\right]\psi(\boldsymbol{r},t). \qquad (1.18)$$

This is a modified Schrödinger equation, with an added non-linearity to account for the inter-particle interactions, and it is the basic equation used to analyze the behavior of Bose-Einstein condensates. The probability density associated to the wave-function is actually a particle density distribution,

$$n(\boldsymbol{r},t) = |\psi(\boldsymbol{r},t)|^2. \qquad (1.19)$$

The ground state of the condensate can be defined when we have stationary solutions that are of the following kind:

$$\psi(\boldsymbol{r},t) = \psi(\boldsymbol{r})e^{-i\mu t/\hbar}, \qquad (1.20)$$

so we get the stationary GP equation,

$$\left[-\frac{\hbar^2}{2m}\nabla^2 + V(\boldsymbol{r}) + g|\psi(\boldsymbol{r})|^2\right]\psi(\boldsymbol{r}) = \mu\psi(\boldsymbol{r}), \qquad (1.21)$$

where the chemical potential can be expressed as

$$\frac{\partial E}{\partial N} = \mu, \qquad (1.22)$$

and can be understood as the energy required to add a particle to the condensate. Notice this expression is identical to the one used in statistical-mechanics.

1.3   The Thomas-Fermi limit

Despite the implementation of certain simplifications, it is convenient to undertake a comprehensive examination of the scenarios in which the Gross-Pitaevskii equation undergoes further simplification. For condensates that are sufficiently large and have repulsive interactions, the limit in which $Na/a_{ho} \gg 1$ becomes relevant. In this regime, the kinetic term of the GP equation, which is proportional to $\nabla^2 \sqrt{n}$ and relates to quantum pressure, becomes negligible. This is known as the Thomas-Fermi (TF) regime, and it is the one used in laboratory conditions for experiments. Making use of this limit, the GP equation can be simplified to the following:

$$\left[V(\boldsymbol{r}) + g|\psi(\boldsymbol{r})|^2 \right] \psi(\boldsymbol{r}) = \mu\psi(\boldsymbol{r}), \tag{1.23}$$

where solving for the density yields

$$n(\boldsymbol{r}) = |\psi(\boldsymbol{r})|^2 = \frac{\mu - V(\boldsymbol{r})}{g}, \tag{1.24}$$

for when $\mu > V(\boldsymbol{r})$, and 0 elsewhere. We can solve for the chemical potential analytically for quadratic potentials. In order to do that, we must remember the normalization condition of Eq. (1.11) and that we may write

$$|\psi(\boldsymbol{r})|^2 = \frac{\mu}{g}\left(1 - \sum_i^3 \frac{m\omega_i^2}{2\mu}r_i^2 \right). \tag{1.25}$$

Therefore,

$$N = \int |\psi(\boldsymbol{r})|^2 d\boldsymbol{r} = \frac{\mu}{g}\int \left(1 - \sum_i^3 \frac{m\omega_i^2}{2\mu}r_i^2 \right) d\boldsymbol{r}. \tag{1.26}$$

Solving the integral in 3 dimensions yields

$$\mu = \frac{\hbar\omega_{ho}}{2}\left(15N\frac{a}{a_{ho}} \right)^{2/5}. \tag{1.27}$$

It is important to mention that the extension condensate in the TF limit can be characterized by its three semi-axes, called the Thomas-Fermi radii, and defined as

$$R_{TF_i} = \sqrt{\frac{2\mu}{m\omega_i^2}} = a_{ho}\left(\frac{\omega_{ho}}{\omega_i} \right)\left(15N\frac{a}{a_{ho}} \right)^{1/5}. \tag{1.28}$$

Unlike in a non-interacting scenario, the Thomas-Fermi radius in each direction exhibits a dependence on the number of particles, so the more particles in the BEC, the larger the Thomas-Fermi radius will be.

1.4   Hydrodynamic formulation

The time dependent GP equation can be rewritten as two coupled differential equations. For this, it is convenient to rewrite the wave-function of the BEC as a function of the density and phase:

$$\psi(\boldsymbol{r},t) = \sqrt{n(\boldsymbol{r},t)}e^{iS(\boldsymbol{r},t)}. \tag{1.29}$$

Using this expression, the velocity field can be obtained, yielding the following:

$$\boldsymbol{v}(\boldsymbol{r}, t) = \frac{\hbar}{m} \nabla S(\boldsymbol{r}, t). \tag{1.30}$$

A full derivation to reach that equation can be seen in [11].

Plugging Eq. (1.29) in the GP Eq. (1.18) we obtain:

- On the left hand side of the GP equation,

$$i\hbar \left(\frac{\partial}{\partial t} \sqrt{n} \right) e^{iS} - \hbar \sqrt{n} \left(\frac{\partial}{\partial t} S \right) e^{iS}. \tag{1.31}$$

- The kinetic term becomes

$$-\frac{\hbar^2}{2m} \nabla [(\nabla \sqrt{n}) e^{iS} + i(\nabla S)\sqrt{n} e^{iS}] = -\frac{\hbar^2}{2m} e^{iS} \left[(\nabla^2 \sqrt{n}) \right. \\ + i(\nabla S)(\nabla \sqrt{n}) + i\left(\nabla^2 S\right) \sqrt{n} + i(\nabla S)(\nabla \sqrt{n}) - (\nabla S)^2 \sqrt{n} \left. \right]. \tag{1.32}$$

- The potential term becomes

$$V\sqrt{n} e^{iS} + gn\sqrt{n} e^{iS}. \tag{1.33}$$

Therefore, equating the real and imaginary parts of the left and right side of the GP equation,

$$\begin{cases} \hbar \dfrac{\partial}{\partial t} \sqrt{n} = -\dfrac{\hbar^2}{2m} \left(2(\nabla \sqrt{n})\nabla S + \sqrt{n}\nabla^2 S \right), \\ -\hbar \sqrt{n} \dfrac{\partial}{\partial t} S = -\dfrac{\hbar^2}{2m} \left(\nabla^2 \sqrt{n} - \sqrt{n}(\nabla S)^2 \right) + V\sqrt{n} + gn\sqrt{n}. \end{cases} \tag{1.34}$$

From the first equation we can derive the continuity equation, which ensures the conservation of the probability:

$$\frac{\partial n}{\partial t} + \nabla(n\boldsymbol{v}) = 0, \tag{1.35}$$

and from the second equation we obtain an equation similar to the hydrodynamic Euler equation for a superfluid, which describes a fluid without viscosity:

$$m\frac{\partial}{\partial t}\boldsymbol{v} + \nabla \left[-\frac{\hbar^2}{2m} \frac{(\nabla^2 \sqrt{n})}{\sqrt{n}} + \frac{1}{2}m\boldsymbol{v}^2 + V + gn \right] = 0. \tag{1.36}$$

The term with $-\left(\hbar^2/2m\right)\left(\nabla^2 \sqrt{n}\right)/\sqrt{n}$ is called the quantum pressure term, and can be neglected in the Thomas Fermi regime due to the electrostatic screening being dominant over the quantum pressure.

Therefore the hydrodynamical formulation of the GP equation reduces to

$$\begin{cases} \dfrac{\partial n}{\partial t} + \nabla(n\boldsymbol{v}) = 0, \\ m\dfrac{\partial \boldsymbol{v}}{\partial t} + \nabla \left(\dfrac{1}{2}m\boldsymbol{v}^2 + V(\boldsymbol{r}, t) + gn \right) = \boldsymbol{0}. \end{cases} \tag{1.37}$$

These two equations will be crucial to investigate non-linear phenomena with a simplified scheme. In fact, they describe very interesting properties of Bose-Einstein condensation, specially the irrotationality of the superfluid, $\nabla \times \boldsymbol{v} = 0$, which will be important in our analysis of rotating condensates.

Chapter 2

Scaling solutions

In this work we will analyze the free expansion of a rotating BEC, using the Thomas-Fermi limit. In order to do that and simulate the evolution of the condensate, there exist self-similar solutions that simplify the hydrodynamic partial differential equations to a system of ordinary differential equations by describing a solution that maintains an overall shape and structure under scaling operations. The goal of this simplification is to ease the numerical computations needed to accurately simulate the desired situation.

Generally, if we use the scaling hypothesis, we predict that the evolution of the density can be given by a scaling coefficient $\lambda(t)$ which is the only term that depends on time, so,

$$n(\boldsymbol{r}, t) = \frac{1}{\prod_j \lambda_j(t)} n_0 \left(\frac{r_i}{\lambda_i(t)} \right), \tag{2.1}$$

where the first term is due to the normalization and each λ_i corresponds to the scaling factor in the axis r_i. It is clear that the spacial dependence is given by r_i but, as mentioned before, $\lambda_i(t)$ describes the time evolution of the BEC, and acts as a scaling factor. In fact, we can complete the hypothesis by substituting the previous expression in the continuity equation to get the scaling for the velocity field

$$v_i(\boldsymbol{r}, t) = \frac{\dot{\lambda}_i}{\lambda_i} r_i. \tag{2.2}$$

Until now no assumptions have been made for the external potential or the initial density profile, so the equations are valid for all situations. We will analyze the cases of a thermal gas and a condensate, to verify the differences.

2.1 Thermal gas

To obtain scaling solutions for a thermal gas, we will consider the non-interacting limit ($g = 0$) for the case in which the condensate is trapped by a harmonic potential. In this situation, the initial density is given by Eq. (1.24), while the scaling solution is given by the following differential equation [10]:

$$\ddot{\lambda}_i(t) = \frac{\omega_i^2(0)}{\lambda_i^3} - \omega_i^2(t)\lambda_i. \tag{2.3}$$

That equation can be easily solved if we take into account that when we release the condensate $\omega_i = 0$, so

$$\omega_i = \begin{cases} \omega_i(0) = \omega_i, & t \leq 0, \\ 0, & t > 0, \end{cases} \tag{2.4}$$

with initial conditions for the scaling parameters being set to $\lambda_i(0) = 1$ and $\dot{\lambda}_i(0) = 0$. It follows that with those initial conditions Eq. (2.3) becomes

$$\ddot{\lambda}_i(t) = \frac{\omega_i^2}{\lambda_i^3}, \tag{2.5}$$

and solving that,

$$\lambda_i(t) = \sqrt{1 + \omega_i^2 t^2}. \tag{2.6}$$

Upon conducting a first analysis on these scaling equations, it is clear that since they are decoupled for all directions, the expansion of each axis will be dependent only on the initial trap frequency in that direction.

2.2 Bose-Einstein condensate

For our case, we will also create the initial shape using a quadratic potential, which will be different in the axial coordinate compared to the z coordinate. We can characterize that potential as

$$V(\boldsymbol{r}, t) \equiv \frac{1}{2} m \omega_{ho}^2 \sum_{ij=1}^{3} x_i W_{ij}(t) x_j, \tag{2.7}$$

where W_{ij} is a symmetric 3×3 matrix. The scaling solution ansatz for the potential above is also quadratic, and using the formulation of the wave-function from Eq. (1.29), we get the following pair of equations:

$$n(\boldsymbol{r}, t) = \frac{m \omega_{ho}^2}{g} \left(n_0(t) - \frac{1}{2} \sum_{i,j=1}^{3} x_i A_{ij}(t) x_j \right), \tag{2.8}$$

$$S(\boldsymbol{r}, t) = m \omega_{ho} \left(s_0(t) - \frac{1}{2} \sum_{i,j=1}^{3} x_i B_{ij}(t) x_j \right). \tag{2.9}$$

Here, A_{ij}, B_{ij}, n_0 and s_0 are the scaling factors. The matrices are also symmetrical due to the properties of the initial potential. These equations are somewhat simplified from the general potential, which may include linear or constant terms, and consequently the solutions would also include linear or constant terms in both the density and the phase. Nevertheless, to set the initial condition we need in this work, the quadratic term is sufficient.

Using this ansatz, we can derive the following ordinary differential equations to simu-

late the expanding condensate,

$$\begin{cases} \dfrac{dn_0}{d\tau} = \text{Tr}(B)\, n_0, \\[2mm] \dfrac{ds_0}{d\tau} = n_0, \\[2mm] \dfrac{dA}{d\tau} = \text{Tr}(B)\, A - \{A, B\}, \\[2mm] \dfrac{dB}{d\tau} = B^2 + W - A, \end{cases} \qquad (2.10)$$

for which $\tau = \omega_{ho} t$. Note that these equations only depend on the initial number of atoms and scattering length through the initial density [13].

The previous derivation is expanded in the Appendix.

Chapter 3

Theoretical description of expanding gases

After getting to know the underlying theory of Bose-Einstein condensation, we will now analyze the situation we are going to investigate more in depth. To do so, it is interesting to define the aspect ratio of the BEC as the ratio between the widths along the axes of the condensate. In particular, for an axially symmetric trap, we define $\omega_\perp \equiv \omega_x = \omega_y$, and the following quantity characterizing the asymmetry of the trap,

$$\lambda = \frac{\omega_z}{\omega_\perp}. \tag{3.1}$$

We will analyze three different situations in order to visualize the interesting properties of rotating BECs. First we are going to see what would happen to a thermal cloud in which a BEC is not formed. After that, a non-rotating condensate will be considered, and lastly the rotating situation will be analyzed.
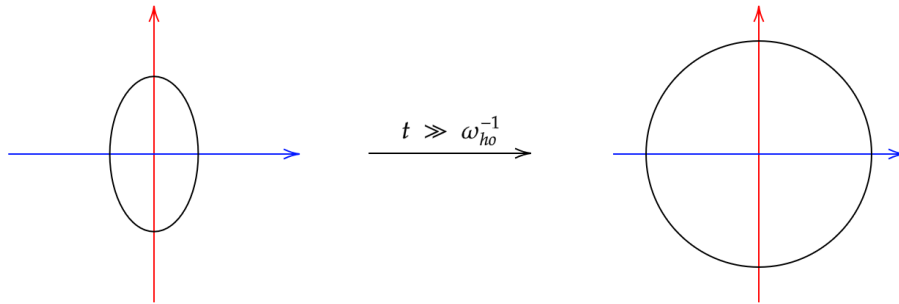
3.1 Thermal Cloud

A thermal cloud, as explained earlier, is formed when the gas is not cold enough to form a Bose-Einstein condensate, namely when the gas is above the critical temperature T_c. Therefore the expansion it follows is a rather simple one. The equations governing its dynamics are, as explained earlier, Eqs. (2.1) and (2.6).

If we set the potential as an axially symmetric quadratic potential, the initial shape of the gas will be a *cigar* shape if $\omega_\perp \gg \omega_z$, and a *disk* shape if $\omega_z \gg \omega_\perp$. We will choose the former one. When we release the cloud, the aspect ratio of the thermal gas during the *time-of-flight* can be computed as [8]

$$AR(t) = \frac{\sqrt{\langle x_z^2(t) \rangle}}{\sqrt{\langle x_\perp^2(t) \rangle}} = \frac{\omega_\perp}{\omega_z} \frac{\sqrt{1 + \omega_z^2 t^2}}{\sqrt{1 + \omega_\perp^2 t^2}}. \tag{3.2}$$

After an asymptotically large time has passed in which $t \gg \omega_{ho}^{-1}$, it is clear that $AR \to 1$, so the thermal gas will be expanded more from the *short* direction. In fact, the expansion on each axis only depends on itself and not the other parameters. Therefore,
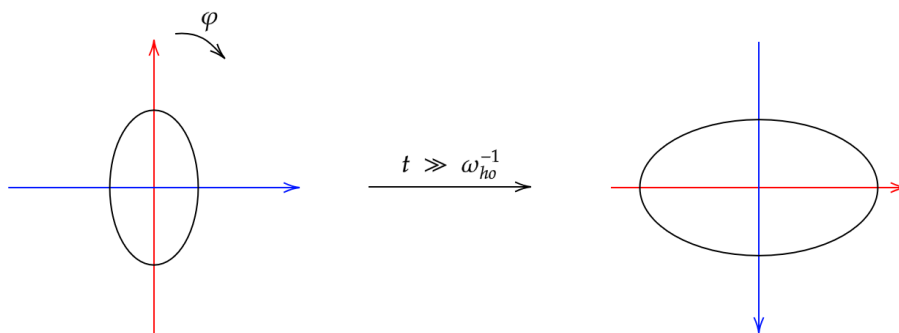
as we can see in Fig. 3.1a, the thermal cloud goes from the cigar shape to an isotropic configuration.

(a) Thermal cloud.
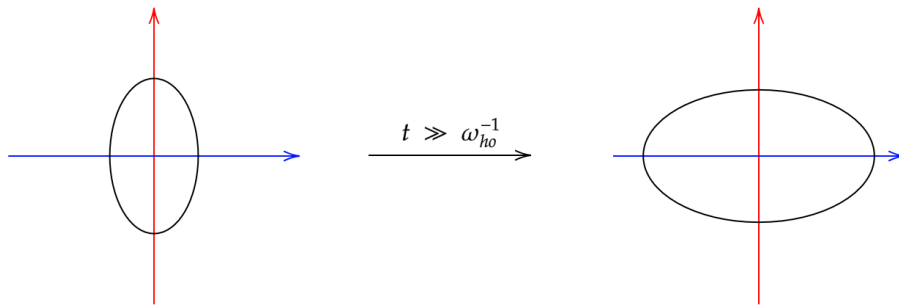
(b) Non-rotating BEC.

(c) Rotating BEC with an angular velocity φ.
Notice the orientation change of the axes.

Figure 3.1: Diagrams of the time evolution of the three cases discussed, initially in a cigar shaped configuration.

3.2 Non-rotating BEC

The starting situation of the BEC is created by an axially symmetric quadratic potential as well. We choose the $y - z$ plane to display and analyze our condensate, even though we shall remember the 3D nature of the condensate. Nevertheless, the analysis for the $x - z$ plane would be identical, and the $x - y$ plane would just display a circular shape due to $\omega_x = \omega_y$

If we release the condensate in this conditions, the expansion will follow these steps:

1. In the beginning, the aspect ratio of the BEC is [8]

$$AR(t = 0) = \frac{1}{\sqrt{\lambda}}. \tag{3.3}$$

2. The condensate will start expanding when we set the potential $V = 0$, and like the normal thermal cloud we have seen before, the BEC will start expanding from the *short* axis faster than the *long axis*.

3. After a long *time-of-flight*, the aspect ratio of the Bose-Einstein condensate becomes $AR = \sqrt{\lambda}$, so it will have passed from a perfectly spherical configuration in which $AR = 1$, and then the *long* and *short* axes will have changed, expanding on the perpendicular direction on a higher rate. An important conclusion in this case is that after the condensate has passed from the vertical shape to an horizontal one, the axis that once was *long* now is the *short* one, while the opposite happens with the axis that was *short* in the initial configuration.

A diagram of the $y - z$ plane projection of the evolution of the non-rotating BEC is shown in Fig. 3.1b, where we can see that the initial *short* axis is the one expanding rapidly.

3.3 Rotating BEC

Now we will see a more interesting situation. Before releasing the condensate from the trap, we will give it an angular velocity, so that when we switch off the potential, it will start expanding while it is rotating. There are some ways to do that operation. Since we have seen that $\boldsymbol{v} = \nabla \boldsymbol{S}/m$, we can set an initial phase that will induce a rotation. Alternatively, a more common way to execute the rotation experimentally is to rotate the potential so that the initial configuration no longer is at the minimum, and hence it will start oscillating around the new potential. Another reason this last one is the most common way of rotating the initial BEC is that we can release it from the trap at different times to analyze the effects under various initial angular velocities. A diagram of the rotated potential and the new minimum configuration can be seen in Fig. 3.2.
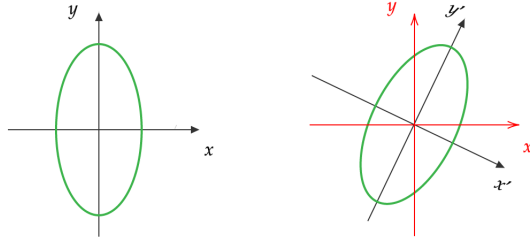
Figure 3.2: Diagram showing the initial configuration of the cigar shaped BEC, and the condensate under rotated potential conditions. In the second diagram the red axes are the original unrotated ones and the black ones (x', y') are the rotated ones. Both BECs are shown in the minimum of the potential.

After letting the condensate turn for some time, we release it from the potential. Due to the lack of potential and the superfluid nature, the energy and angular momentum must be conserved, so while the initial evolution is very similar to a non rotating condensate but with a rotation, things change as soon as the aspect ratio approaches unity.

The moment of inertia of a BEC is given by

$$\Theta = \frac{\langle x^2 - y^2 \rangle^2}{\langle x^2 + y^2 \rangle^2} \Theta_{rig}, \tag{3.4}$$

where Θ_{rig} is the rigid body value. We see that the real moment of inertia is quenched or deformed with respect to the rigid body. It is clear from that equation that the moment of inertia of the rotating BEC will be zero when it has a cylindrical symmetry. Due to the peculiarity of the superfluid and the conservation of energy and angular momentum, if the Bose-Einstein condensate is rotating, Θ cannot be 0. Therefore, in order not to break conservation laws, the spatial configuration never reaches cylindrical symmetry and the the aspect ratio, although close, never reaches unity. What happens is that close to this situation, the condensate performs a rapid rotation so that the initial *long* axis is now perpendicular to the initial configuration and is the one that keeps expanding [13] [14]. This will be better understood once the simulations and numerical results are presented.

Therefore, to sum up all three cases, for a thermal cloud an isotropic spherical configuration will be achieved for asymptotically large times; for a non-rotating BEC the *long* axis and the *short* axis will switch and the expansion after some time has passed will be in the opposite direction from the initial long axis; and for a rotating BEC, the axes will not be switched and even though it would seem that the final configuration is the same as in the non-rotating case, this time the *long* axis will be the one expanding after a fast rotation. The three cases can be visualized in Fig. 3.1.

16

Chapter 4

Numerical solutions

Now that we have understood the problem and have had an in depth view of the theoretical evolution the condensate should have, we shall proceed to analyze the numerical solutions of the simulated the gas. We will divide this section in two parts: the first one will show that, as described above, the thermal cloud will lead to an spherical configuration, and after that we will look at the evolution of the condensate. The numerical methods used in the calculations are explained in the Appendix.
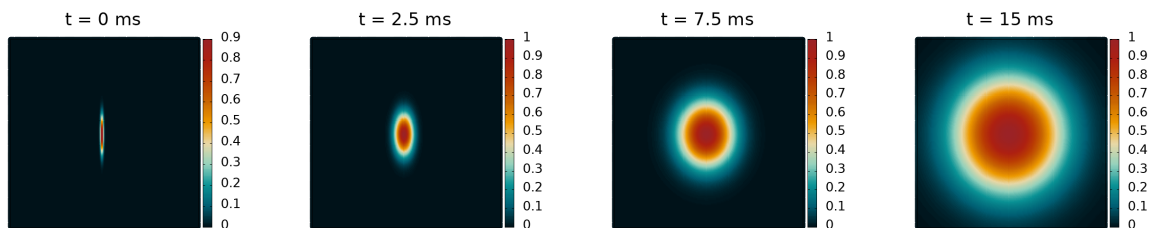
4.1 Thermal cloud

The simulations of the thermal cloud are pretty straightforward. Since we are only interested in a qualitative view of the dynamical evolution of the thermal cloud, we are permitted to simulate a generic gas with arbitrary initial conditions.

We will take the initial configuration of the gas to be that of the *cigar* shaped, and to model that we will use a Gaussian function:

$$n_0(\boldsymbol{r}, 0) = e^{-x^2-y^2-\lambda^2 z^2}, \qquad \lambda = \frac{\omega_z}{\omega_\perp}. \tag{4.1}$$

The results can be seen in Fig. 4.1, where we take $\lambda = 16.3/200$ to have the same conditions as in the following sections. It is clear that what was theoretically described is correct. The thermal cloud begins in a very elongated shape but after 15 ms it has the characteristic symmetrical configuration in which $AR \approx 1$ and if we let it expand for a longer time, it will asymptotically reach the expected aspect ratio $AR \equiv 1$.

Figure 4.1: Frames of the distribution of a thermal cloud. Axes are arbitrarily normalized in order to ease visualization. The density is normalized to the value of the origin.

4.2 Bose-Einstein condensate

There are other interesting calculations to be made besides the dynamics of the density of the condensate. Mainly, we will focus on the angle of rotation, the visualization of the main axes of the BEC and its aspect ratio. To calculate these parameters, it is of utmost importance the correct representation of the density with the matrix A we have in Eq. (2.8).

Before beginning with the simulation, the initial condition for the density must be determined by setting $A_{11} = A_{22} < A_{33}$. The exact values to be used are $A_{11} = A_{22} = 1.0$ and $A_{33} = \lambda^2$ (recall Eq. (3.1)), and this will create the *cigar* shape. Then, we will set the initial potential. It is crucial for the matrix W to have the same values as A before the rotation in order to avoid deformations on the condensate before the free expansion. These would be caused by the shifted position of the BEC with respect to the minimum state of the potential.

After having our matrices set, we apply the RK-4 method with a timestep of $dt = 0.025$ ms. The smaller dt, the lower the error will be.

The simulations will be made in order to replicate the experiments done in [13]; thus, the values of the initial density will be set using the values for ^{87}Rb atoms, with the anharmonicity of $\omega_z = 2\pi \times 16.3$ Hz and $\omega_\perp = 2\pi \times 200$ Hz.

4.2.1 Non-rotating BEC

Now that we have described the initial configuration to be used, we will first consider turning off the trap at $t = 0$, effectively not rotating the condensate and therefore analyzing that situation. Various frames of this simulations are shown in Fig. 4.2. There we can see that the axes (represented by the colored lines) do not rotate and it has no problems to pass the $AR = 1$ position to further expand from the short axis. Therefore, in this case, the theoretical description matches the computational results.
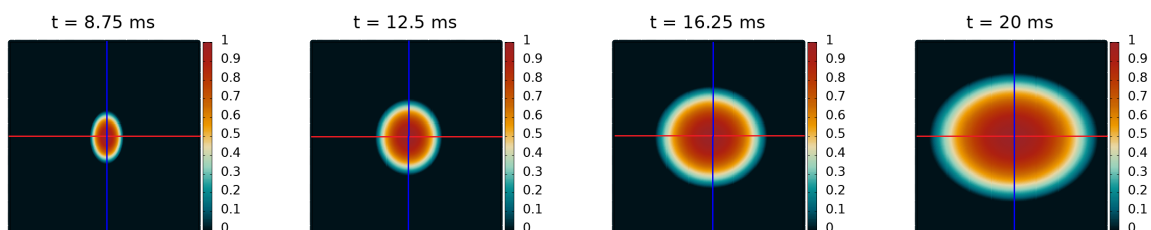
Figure 4.2: Frames of the distribution of a expanding non-rotating BEC. Axes are arbitrarily normalized in order to ease visualization and the density is normalized the value of the origin. The red and blue lines represent the *initial* long and short axes, respectively. Notice that asymptotically the BEC becomes elongated along the direction in which it is initially more confined.

4.2.2 Rotating BEC

We are interested in analyzing the effect of the fast rotation, and therefore simulations will be made for four different initial angular velocities for each angle θ we rotate the potential. For that we will release the BEC at different times. The first one will be after $t = 0.125$ ms, when the release angular velocity φ is still very small; the second one will be at $t = 0.625$ ms; the third one will be at 1.25 ms, which is when the condensate is close to the minimum of the potential and therefore has its maximum velocity; and the last one will be made at $t = 2.5$ ms, which is when the condensate has a very small velocity at the other side of the potential. We can see the evolution of the condensate under the rotated potential in Fig. 4.3, where each point represents a different release time and thus a different velocity. It is also clear the oscillatory nature of the evolution under the potential.
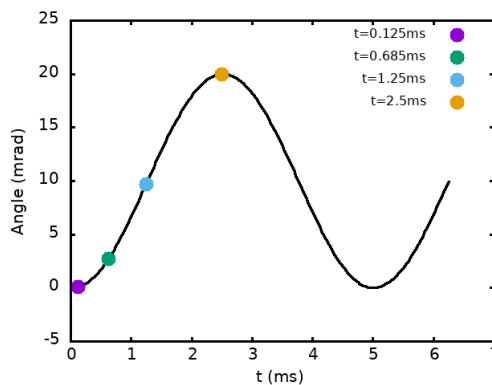

Figure 4.3: Evolution of the angle of the condensate with respect to the original axis as a function of time, and different release times when the potential minimum is at $\theta = 10$ mrad.

For a clear view of what is happening with the rotating BEC, Figs. 4.4 and 4.5 show different instances of the condensate on the $y - z$ plane released at 0.625 ms and 1.25 ms. The frames are all separated by 1.375 ms, and we have decided to omit the initial pictures so as to center on the timespace in which the rapid rotation happens. The values have been normalized, but in reality the expansion is significant. In the first frame in which the BEC is released, its *long* axis length is around 100 μm, while at the end it has expanded by more than three orders of magnitude. We believe that the visualization is easier if the axes of the figures are fixed at an arbitrary value and the condensate is normalized. We clearly see an expansion but it does not reflect reality with precision. Besides, the density $n(\boldsymbol{r}, t)$ has been normalized to its center value $n_0 = n(\boldsymbol{0}, t)$, which starts at $n_0 \sim 10^{-13}$ kg m^{-3} and ends at $n_0 \sim 10^{-15}$ kg m^{-3}.
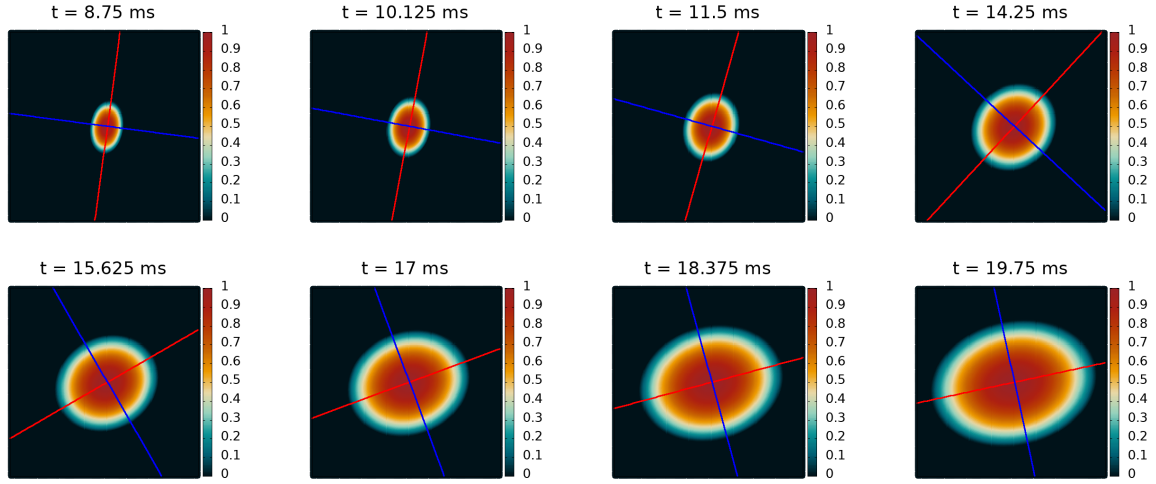
Figure 4.4: Frames of the distribution of the BEC density at different times when released at $t = 0.625$ ms. The blue line represents the orientation of the *short* axis while the red one represents the *long* one. Spatial axes are arbitrarily normalized to ease visualization ans the density is normalized to that of the central value.
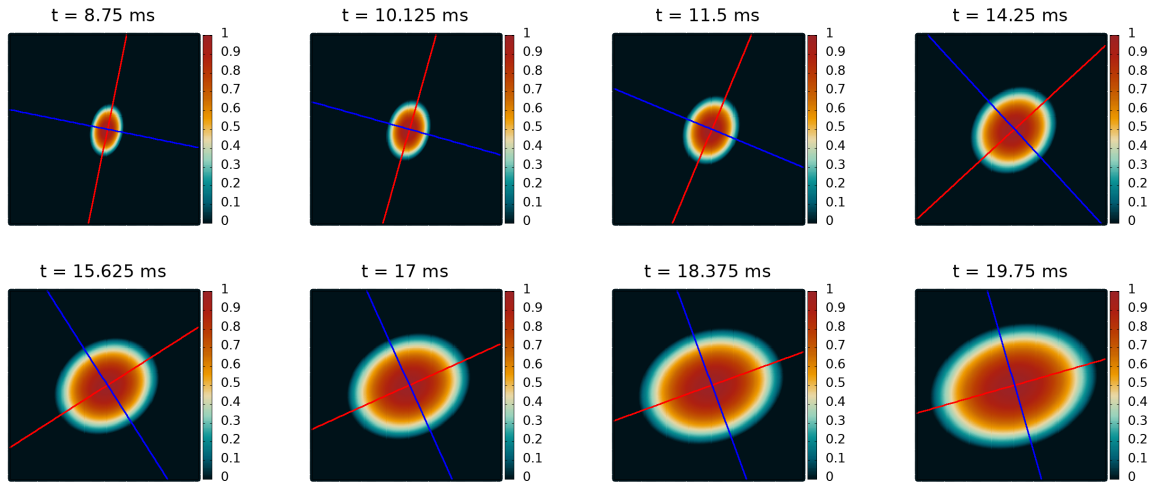

Figure 4.5: Frames of the distribution of the BEC density at different times when released at $t = 1.25$ ms. The blue line represents the orientation of the *short* axis while the red one represents the *long* one. Spatial axes are arbitrarily normalized to ease visualization ans the density is normalized to that of the central value.

The previous figures clearly show a fast rotation occurring around $13 - 15$ ms. To have an in depth view of this phenomenon, in Fig. 4.6 we present the aspect ratios and angles for the release times specified in Fig. 4.3, and therefore for different initial angular velocities. The analysis will be done with three rotation angles for the initial potential: $\theta = 0.005,\ 0.01,\ 0.1$ rad.
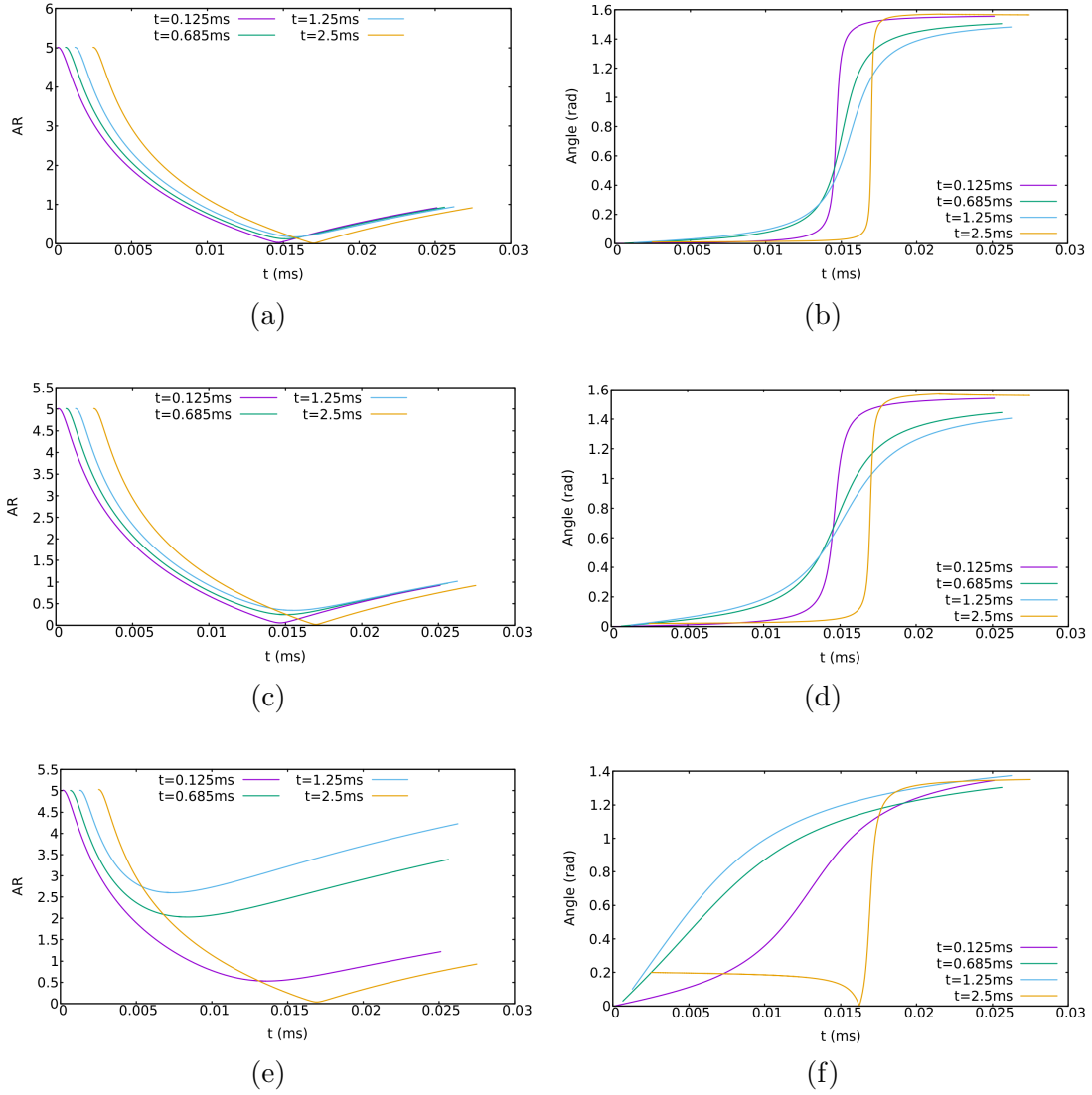
Figure 4.6: Aspect ratios in a logarithmic scale and angles of the rotating BEC with the rotated potential at $\theta = 0.005$, 0.01, 0.1 rad respectively in each row, for different release times as a function of time.

Let us discuss the results. First of all, qualitatively the results for the angles $\theta = 0.005$ rad and $\theta = 0.01$ rad seem similar. It is very clear that the bigger the initial angular velocity, the smaller the effect will be. This is due to the fact that the BEC needs to reach the 90° rotation, and if the initial angular velocity is bigger it will reach the final state faster so it does not need to rotate at a higher velocity. It is also true that for those high angular velocity releases, the aspect ratio is not too close to the forbidden symmetrical shape. On the contrary, the smaller the initial angular velocity the closer it gets to $AR = 1$, so it needs to rapidly rotate in order to avoid it. Therefore, when the aspect ratio reaches its minimum value (even though it never reaches 0 in the log scale) the angular velocity is maximum.

Looking at Figs. 4.6e and 4.6f, it is clear the behavior of the BEC is different. In this case we have 3 kinds of evolution. When the condensate is released early, even though it has a smaller φ than the $t = 0.625$ ms and $t = 1.25$ ms releases, the effect is quite small.

This is because the potential angle is much larger than in Figs. 4.6a, 4.6b and 4.6c, 4.6d, so it never gets too close to $AR = 1$ and the angular velocity does not have a spike. When we release the BEC after more time, we clearly see that there is no rapid rotation and we cannot see the effect described earlier: the condensate has enough angular velocity to turn 90° faster than it gets close the critical aspect ratio so there is no need for a fast rotation, and φ is reduced in a gradual manner. This effect is also described in [14]. Lastly, it is interesting to review what happens when we release the BEC at $t = 2.5$ ms. Here it has already reached the angle 2θ by the time we release it, so the angular velocity is reversed and it goes through 0 before rotating the other way, again, rapidly.

Another interesting phenomenon worth mentioning is that after the fast rotation has been performed, the condensate approaches the angle $\theta = \pi/2$ rad asymptotically. The rotation must continue but as the angular momentum has to be conserved, due to the expansion of the BEC the angular velocity tends to zero. This happens after the rotation has been performed because even though the condensate is always growing, the expansion of the *short* axis compensates the one of the *long* one in the beginning, so it is only when it stops expanding from the *short* axis that the BEC expands extremely rapidly and the velocity decreases drastically.
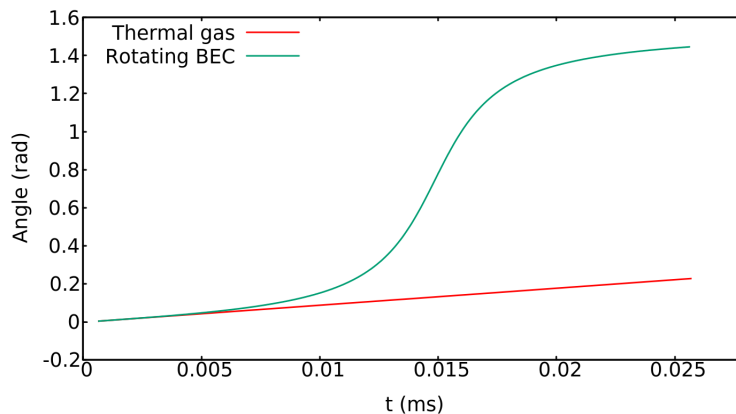
Figure 4.7: Comparison between a rotating BEC and a rotating thermal cloud, in the case of $\theta = 0.01$ and release at $t = 1.25$ ms.

Comparing this behavior with the one of the thermal cloud, in Fig. 4.7 it appears that both the rotating BEC and the gas have the same trend during the slow rotating phase, but when the aspect ratio gets close to unity, the rotating thermal cloud does not change its rotation rate and keeps going almost linearly. Therefore, it is clear that this rapid rotation effect happens only in Bose-Einstein condensates.

22

Conclusions

The goal of this thesis has been to analyze the intriguing behavior of a superfluid BEC when it is released from a harmonic trap with an angular velocity, and to compare it to a non-rotating case and a thermal cloud.

As our most important conclusion, we have specially focused on the case for the rotating BEC, in which the effects of superfluidity are clear. We have investigated the rapid rotation it undergoes in order to avoid breaking the conservation of energy and angular momentum. Since those conservation laws cannot be broken and the moment of inertia of a rotating Bose-Einstein condensate is quenched comparing it with the value of the rigid body, a symmetrical configuration is not possible as it would render the moment of inertia to be zero. This phenomenon only happens due to the fact that Bose-Einstein condensates exhibit superfluid properties and the rotation.

In order to execute this work, several steps have been undertaken:

1. First of all, acquiring a basic knowledge of the mathematical formalism of Bose-Einstein condensation has been a prerequisite. That includes the understanding of the Gross-Pitaevskii equation, the hydrodynamic formulation of the GP equation, and the non-interacting and Thomas-Fermi limits.

2. A set of ordinary differential equations have been derived to ease the complexity of simulating the condensate using directly the GP equation. In order to do that, we have had to understand the self-similar or scaling solutions and successfully apply them to the harmonic potential we have used.

3. An initial description of the phenomena occurring has been made based on the formalism explained in the first two chapters, and the evolution of each case has been theorized as well as their differences.

4. A program has also been written to calculate various parameters for the cases of the thermal cloud and the rotating and non-rotating condensates using the direct scaling solution for the first case and the numerical iterative method Runge-Kutta of 4th order for the others. We have also created various figures to ease the understanding of the phenomena happening.

Besides the main effect, we have also found more interesting outcomes. Firstly, the theoretical part has been specially useful to understand the underlying physics of a Bose-Einstein condensate, and therefore the reasoning behind the superfluidity they can exhibit and the effects we have observed.

Moreover, in the case of the rotating BEC the fact that it reaches an asymptotic angle due to the expansion has been verified. We have outlined the differences of that case with

a thermal cloud and seen that even though the in the first instances the evolution seems similar it changes after the condensate gets close to a symmetrical configuration. We have also mentioned the differences of the BEC being rotating or not and how that affects to its expansion.

Lastly, although the case for the thermal cloud has been a more qualitative result rather than an exact reproduction of experiments, the cases for the BEC, both the rotating and non-rotating case, recreate the results obtained in previous experiments such as the one described in [13]. They accurately describe the singular phenomena occurring in rotating condensates.

Appendix A

Mathematical derivations and code snippets

A.1 Self-similar solutions of the hydrodynamic equations

We are going to derive the ODEs mentioned as the evolution of scaling solutions for BECs, namely Eq. (2.10). We shall take the hydrodynamic equations for the Thomas-Fermi regime as our basic equations,

$$
\begin{cases}
\dfrac{\partial n}{\partial t} + \dfrac{1}{m}\nabla\left(n\nabla S\right) = 0, \\
\dfrac{\partial S}{\partial t} + \dfrac{1}{2m}\left(\nabla S\right)^2 + V + gn = 0.
\end{cases}
\tag{A.1}
$$

Calculating the spatial derivative of the ansatz Eqs. (2.8) and (2.9),

$$
\begin{cases}
\partial_{x_k} n = -\dfrac{m\omega_{ho}^2}{g}\displaystyle\sum_i x_i A_{ik}, \\
\partial_{x_k} S = -m\omega_{ho}\displaystyle\sum_i x_i B_{ik}.
\end{cases}
\tag{A.2}
$$

Therefore, we can calculate each part of Eq. (A.1). Since $\nabla(n\nabla S) = \nabla n \cdot \nabla S + n\nabla^2 S$, we get

$$
\begin{cases}
\nabla n \cdot \nabla S = \dfrac{m^2\omega_{ho}^3}{g}\displaystyle\sum_{ij=1}^{3} x_i(A\cdot B)_{ij}x_j, \\
\nabla^2 S = -m\omega_{ho}\displaystyle\sum_i B_{ii} = -m\omega_{ho}\,\mathrm{Tr}(B), \\
n\nabla^2 S = -\dfrac{m^2\omega_{ho}^3}{g}\,\mathrm{Tr}(B)\left(n_0 - \dfrac{1}{2}\displaystyle\sum_{ij=1}^{3} x_i A_{ij}x_j\right).
\end{cases}
\tag{A.3}
$$

Now substituting in the first Eq. (A.1) and simplifying terms,

$$\left(\dot{n}_0 - \frac{1}{2} \sum_{ij=1}^{3} x_i \dot{A}_{ij} x_j \right) +$$

$$\omega_{ho} \left(\sum_{ij=1}^{3} x_i (A \cdot B)_{ij} x_j - \text{Tr}(B) \left[n_0 - \frac{1}{2} \sum_{ij=1}^{3} x_i A_{ij} x_j \right] \right) = 0. \quad \text{(A.4)}$$

Since the matrices A and B are symmetrical, if we write $(A \cdot B) = \frac{1}{2}[A, B] + \frac{1}{2}\{A, B\}$, the first term that indicates the commutation of the matrices is equal to 0, so it simplifies to the anticommutation term.

If we now focus on the second expression of Eq. (A.1), using the equations we got earlier and simplifying,

$$\left(\dot{s}_0 - \frac{1}{2} \sum_{ij=1}^{3} x_i \dot{B}_{ij} x_j \right) + \frac{\omega_{ho}}{2} \left(\sum_{ij=1}^{3} x_i B_{ij}^2 x_j \right)$$

$$+ \frac{\omega_{ho}}{2} \left(\sum_{ij=1}^{3} x_i W_{ij} x_j \right) + \omega_{ho} \left(n_0 - \frac{1}{2} \sum_{ij=1}^{3} x_i A_{ij} x_j \right) = 0. \quad \text{(A.5)}$$

Equalling the matricial parts and the scalars separately, and defining a new variable $\tau = \omega_{ho} t$, we have gone from the GP equation to the hydrodynamic equations in the first chapter, and from there we have simplified our problem from 2 PDEs to 4 coupled ODEs (in reality we have one ODE for each value i, j in the matrices A and B):

$$\begin{cases} \dfrac{dn_0}{d\tau} = \text{Tr}(B) \, n_0, \\[2mm] \dfrac{ds_0}{d\tau} = n_0, \\[2mm] \dfrac{dA}{d\tau} = \text{Tr}(B) \, A - \{A, B\}, \\[2mm] \dfrac{dB}{d\tau} = B^2 + W - A. \end{cases} \quad \text{(A.6)}$$

A.2   A brief explanation of the Runge-Kutta method

Since we are dealing with ODEs, one of the most efficient ways to calculate the time evolution of the condensate is using the Runge-Kutta 4 (RK-4) iterative method. To use an iterative method such as Runge-Kutta, the initial value of the function $y(t)$ has to be known and its time evolution needs to be described as

$$\frac{dy}{dt} = f(t, y). \quad \text{(A.7)}$$

Therefore, we need to know $f(t, y)$, t_0 and $y(t_0)$. From there, the method consists on discretising the time derivative into finite timesteps. The simplest RK method called the Euler method is the most straightforward to explain. Since the initial conditions are

known and the derivative is defined as f, if a small timestep h is taken the new value for $y_1(t_1)$ will be close to the real value. Therefore, the full method for t_{i+1} will be

$$\begin{cases} t_{i+1} = t_i + h, \\ y_{i+1} = y_i + hf(t_i, y). \end{cases} \tag{A.8}$$

This method can be proven by using the Taylor expansion of the function y,

$$y(t_0 + h) = y(t_0) + h\dot{y}(t_0) + O(h^2) \tag{A.9}$$

If we ignore the terms of order h^2 or higher, and since we know that $\dot{y} = f(t, y)$, we recover Eqs. (A.8).

It is straightforward to see how the total error in this method is $O(h)$ due to the fact that the number of steps taken depends on $1/h$ and the truncating error on the Taylor expansion is $O(h^2)$. This error is too large for a simulation with almost 1000 steps as we will be performing.

To reduce the error in our calculation, we shall proceed with the RK-4 method. From a theoretical point of view it is pretty similar to the Euler method explained earlier but this time, terms up to the order $O(h^5)$ are taken into account from the Taylor expansion, so the total error $O(h^4)$ is much lower than in the one explained earlier [15]. This method can be explicitly written as

$$\begin{cases} t_{i+1} = t_i + h, \\ y_{i+1} = y_i + \dfrac{h}{6}(k_1 + 2k_2 + 2k_3 + k_4), \end{cases} \tag{A.10}$$

where,

$$\begin{cases} k_1 = f(t_i, y_n), \\ k_2 = f\left(t_i + \dfrac{h}{2}, y_i + h\dfrac{k_1}{2}\right), \\ k_3 = f\left(t_i + \dfrac{h}{2}, y_i + h\dfrac{k_2}{2}\right), \\ k_4 = f\left(t_i + \dfrac{h}{2}, y_i + hk_3\right). \end{cases} \tag{A.11}$$

In our case, since we are dealing with 4 coupled ODEs, we shall calculate k_i for each step in order: first k_1 for all our ODEs, then k_2, ... The following code demonstrates how it can be implemented in Fortran 90. This coding language has been chosen due to its fast calculations and easy matrix manipulation[1].

---

[1]The full program will not be included, just snippets of relevant code.

```fortran
subroutine rk4(t, y, h, W)
  implicit none
  real(kind=dp), dimension(7,3), intent(inout)    :: y
  real(kind=dp), intent(inout)                     :: t
  real(kind=dp), intent(in)                        :: h
  real(kind=dp), dimension(3,3), intent(in)        :: W
  real(kind=dp), dimension(7,3)                    :: k1, k2, k3, k4, &
 y_ph

  call deribatu(y, W, k1)
  y_ph(:,:) = y(:,:)+0.5*h*k1(:,:)
  call deribatu(y_ph, W, k2)
  y_ph(:,:) = y(:,:)+0.5*h*k2(:,:)
  call deribatu(y_ph, W, k3)
  y_ph(:,:) = y(:,:)+h*k3(:,:)
  call deribatu(y_ph, W, k4)

  y(:,:) = y(:,:)+(h/6.0)*(k1(:,:)+2*k2(:,:)+2*k3(:,:)+k4(:,:))
end subroutine rk4

subroutine deribatu(y, W, dy)
  implicit none
  real(kind=dp), dimension(7,3), intent(in)     :: y
  real(kind=dp), dimension(3,3), intent(in)     :: W
  real(kind=dp), dimension(7,3), intent(out)    :: dy
  real(kind=dp), dimension(3,3)                 :: A, B, dA, dB, &
 anticommutator, B2
  real(kind=dp)                                 :: rho0, drho0, s0, &
 ds0, tr_b

  tr_b = 0.0
  A(:,:) = y(1:3,:)
  B(:,:) = y(4:6,:)
  rho0 = y(7,1)
  s0 = y(7,2)

  tr_b = B(1,1)+B(2,2)+B(3,3)
  anticommutator = matmul(A,B)+matmul(B,A)
  B2 = matmul(B,B)

  drho0 = (rho0*tr_b)
  ds0 = rho0

  dA(:,:) = (2.0_dp*tr_b*A(:,:)+anticommutator(:,:))
  dB(:,:) = (W(:,:)-A(:,:)+B2(:,:))

  dy(1:3,:) = dA(:,:)
  dy(4:6,:) = dB(:,:)
  dy(7,1) = drho0
  dy(7,2) = ds0
  dy(7,3) = 0.0
end subroutine deribatu
```

Notice the subroutine *deribatu* contains the differential equations Eq. (2.10), while the subroutine *RK4* calculates each timestep. The vector y has all relevant information about the previous iteration.

A.3 Rotated potential and condensate eigenaxes

Even though the matrix A is symmetrical during the whole expansion, in the beginning it is diagonal, with each eigenvector representing the direction of the axes and with the eigenvalues representing how *deformed* it is in each direction. When the condensate starts rotating, A_{23} and A_{32} will start having non zero values. With that in mind, to know the direction of the *long* and *short* axes, we will have to diagonalize A each iteration, and to know the angle we will just have to calculate the arc-tangent between the eigenvectors. To do so is straightforward, since all symmetrical matrices are diagonalizable and we are only interested in the $y - z$ plane so we need to perform the operation on the 2x2 matrix

$$\begin{pmatrix} A_{22} & A_{23} \\ A_{32} & A_{33} \end{pmatrix}. \tag{A.12}$$

The following code is an example of how the diagonalization can be made.

```fortran
subroutine diag(matrix, eigenvalues, eigenvectors)
  implicit none
  real(kind=dp), dimension(2,2), intent(inout)  :: matrix(2,2)
  real(kind=dp), dimension(2), intent(out)      :: eigenvalues(2)
  real(kind=dp), dimension(2,2), intent(out)    :: eigenvectors(2,2)
  real(kind=dp) :: tr, det, ph

  eigenvectors(1,:) = 1.0

  tr = matrix(1,1) + matrix(2,2)
  det = matrix(1,1) * matrix(2,2) - matrix(1,2) * matrix(2,1)

  eigenvalues(1) = (tr + sqrt(tr**2 - 4.0 * det)) / 2.0
  eigenvalues(2) = (tr - sqrt(tr**2 - 4.0 * det)) / 2.0

  eigenvectors(2,1) = (eigenvalues(1) - matrix(2,2)) / matrix(2,1)
  eigenvectors(2,2) = (eigenvalues(2) - matrix(2,2)) / matrix(2,1)

  ph = sqrt(eigenvectors(1,1)**2 + eigenvectors(2,1)**2)
  eigenvectors(:,1) = eigenvectors(:,1) / ph

  ph = sqrt(eigenvectors(1,2)**2 + eigenvectors(2,2)**2)
  eigenvectors(:,2) = eigenvectors(:,2) / ph
end subroutine diag
```

Besides, we need to turn the potential matrix for the condensate to start rotating. Once the initial W matrix has been set, we will rotate it some angle θ. To do this, we will perform the following operation:

$$R^T W R = \begin{pmatrix} 1 & 0 & 0 \\ 0 & \cos\theta & \sin\theta \\ 0 & -\sin\theta & \cos\theta \end{pmatrix} \begin{pmatrix} W_{11} & 0 & 0 \\ 0 & W_{22} & 0 \\ 0 & 0 & W_{33} \end{pmatrix} \begin{pmatrix} 1 & 0 & 0 \\ 0 & \cos\theta & -\sin\theta \\ 0 & \sin\theta & \cos\theta \end{pmatrix}. \tag{A.13}$$

Using the values for $W_{11} = W_{12} = 1$ and $W_{33} = \lambda^2$, which are the ones set in the matrix A as well, we obtain

$$\begin{pmatrix} 1 & 0 & 0 \\ 0 & \cos^2\theta + \lambda^2\sin^2\theta & \sin\theta\cos\theta(1-\lambda^2) \\ 0 & \sin\theta\cos\theta(1-\lambda^2) & \sin^2\theta + \lambda^2\cos^2\theta \end{pmatrix}. \tag{A.14}$$

It is clear that the rotated matrix maintains the symmetric shape of the initial matrix W, and therefore so will the matrix A during the time evolution and the expansion.

Bibliography

[1] M. Modugno, Exploring the quantum world with ultracold atoms (2016).

[2] R. P. Feynman, Rev. Mod. Phys. **29**, 205 (1957).

[3] S. Bose, Zeitschrift für Physik **26**, 178 (1924).

[4] A. Einstein, Quantentheorie des einatomigen idealen gases (1924).

[5] M. H. Anderson, J. R. Ensher, M. R. Matthews, C. E. Wieman, and E. A. Cornell, Science **269**, 198 (1995).

[6] K. B. Davis, M. O. Mewes, M. R. Andrews, N. J. van Druten, D. S. Durfee, D. M. Kurn, and W. Ketterle, Phys. Rev. Lett. **75**, 3969 (1995).

[7] A. O. Jamison, J. N. Kutz, and S. Gupta, Phys. Rev. A **84**, 043643 (2011).

[8] M. Modugno, An introduction to the theory of bose-einstein condensation in trapped gases (2016).

[9] F. Dalfovo, S. Giorgini, L. P. Pitaevskii, and S. Stringari, Theory of Bose-Einstein condensation in trapped gases (1998).

[10] L. Pitaevskii and S. Stringari, Bose-Einstein condensation and superfluidity (2016).

[11] C. J. Pethick and H. Smith, *Bose–Einstein Condensation in Dilute Gases*, 2nd ed. (Cambridge University Press, 2008).

[12] A. J. Leggett, Rev. Mod. Phys. **73**, 307 (2001).

[13] M. Modugno, G. Modugno, G. Roati, C. Fort, and M. Inguscio, Phys. Rev. A **67**, 4 (2003).

[14] M. Edwards, C. W. Clark, P. Pedri, L. Pitaevskii, and S. Stringari, Phys. Rev. Lett. **88**, 704051 (2002).

[15] W. H. Press, S. A. Teukolsky, W. T. Vetterling, and B. P. Flannery, *Numerical Recipes 3rd Edition: The Art of Scientific Computing*, 3rd ed. (Cambridge University Press, 2007).